

Investigating non-Keplerian motion in flare events with astrometric data

Fengting Xie,^{*} Qing-Hua Zhu,[†] and Xin Li[‡]

School of Physics, Chongqing University, Chongqing 401331, China

The GRAVITY interferometer has achieved microarcsecond precision in near-infrared interferometry, enabling tracking of flare centroid motion in the strong gravitational field near the Sgr A*. It might be promising to serve as a unique laboratory for exploring the accretion matter near black holes or testing Einstein's gravity. Recent studies debated whether there is a non-Keplerian motion of the flares in the GRAVITY dataset. It motivates us to present a comprehensive analysis based on error estimation under the Bayesian framework. This study uses astrometric flare data to investigate the possibility that the flares exhibit deviations from the circular Keplerian motion. By fixing the black hole mass of Sgr A* and using the averaged astrometric data from the four flares, our results find that the super-Keplerian orbit is favored at the near 1σ confidence level, where the non-Keplerian parameter is $\omega/\omega_k = 1.45^{+0.35}_{-0.38}$. By treating the black hole mass as a free parameter, both the averaged and individual data exhibit no significant evidence in favor of non-Keplerian motions, where the non-Keplerian parameter is close to 1 within 1σ confidence level. We further analyze flares undergoing planar geodesic motion, where the orbital circularity parameter is $\gamma = 0.99^{+0.07}_{-0.10}$. This indicates that the astrometric data favor the circular orbits. Future improvements in astrometry precision might enable stronger constraints on the kinematical behavior of the flares, potentially offering insights into black hole physics or accretion matter in the strong-field regime.

I. INTRODUCTION

In weak field regime of gravity, pioneers' studies have confirmed the validity of general relativity to a certain extent [1–6], including classical experiments such as the Shapiro time delay [1], constraints on parametrized post-Newtonian (PPN) parameters [2], as the gravitational redshift and Schwarzschild precession observed in the orbit of the S2 star [3, 4]. The relativistic effect is necessary because the observations can not be fully explained by Newtonian gravity alone.

In the strong gravitational field regime, the closest known supermassive black hole (SMBH) at the center of our galaxy, namely, Sagittarius A* (Sgr A*), might serve as a unique laboratory for exploring the accretion matter near the black holes and testing Einstein's gravity [7–10]. The

^{*} xiefengting@stu.cqu.edu.cn

[†] zhuqh@cqu.edu.cn (corresponding author)

[‡] lixin1981@cqu.edu.cn

supermassive black hole with a mass of $M = 4.3 \times 10^6 M_\odot$ [11] and a distance of $D = 8.178 \text{ kpc}$ [12] has been the focus of continuous observation over the past decades [10]. In 2022, the Event Horizon Telescope (EHT) Collaboration released the first image of Sgr A* [13, 14], reconstructed using very-long-baseline interferometry (VLBI). The image revealed the potential shadow of the black hole and provided a support for the validity of general relativity at the event horizon scale [15–23].

With the advancement of observational techniques, the GRAVITY Collaboration has achieved microarcsecond precision in near-infrared interferometry, enabling tracking of flare centroid motion in the strong gravitational field near the Sgr A* [24–26]. The GRAVITY interferometer, installed at the Very Large Telescope (VLT), is dedicated to high-precision monitoring of the Galactic Center black hole and reported its detection of flares from Sgr A* in 2018 [25]. These data include both astrometric positions and polarization measurements. Subsequently, the GRAVITY Collaboration updated the dataset of the Sgr A* flares, reporting four flares with astrometric measurements and six with polarimetric data [26]. Notably, two of flares were well covered in both domains. All astrometric measurements revealed a consistent clockwise motion of the flare centroids on the sky with periods of approximately one hour, accompanied by full rotations of the polarization vector at the same time. The astrometric positions of these flares are located very close to the Galactic Center, within a few Schwarzschild radii, implying that general relativity’s strong-field predictions could be tested.

The flares might physically originate from the dynamics of accretion matter in the vicinity of the center black hole [27, 28]. Its phenomenological behavior could be described as a compact blob of plasma orbiting near the innermost stable circular orbit (ISCO), referred as to hotspot model [29–41]. Based on GRAVITY datasets, Refs. [42, 43] explored various kinematic scenarios for flare motion. Notably, Ref. [43] showed that super-Keplerian orbits often provide a better match to the observations. Via fitting the flare astrometric data, GRAVITY Collaboration reported that while centroid motion is generally consistent with a circular orbit, the observed orbital period is shorter than the predicted Keplerian period [44]. Further studies by Ref. [45] provided additional support for the super-Keplerian interpretation. However, Refs. [25, 26] still emphasized that the flare motions remain consistent with a standard Keplerian model.

Motivated by this tension, this paper analyzes the flare data released by the GRAVITY Collaboration in 2023, and performs hotspots’ orbit fitting for the four flares in the Bayesian parameter estimation framework. The astrometric data of the four flare events can also be averaged, due to the similarity between the flares [26]. We will separately analyze the averaged and individual

data with the error estimation and provide a comparison of the results. We also study non-circular motion of the flares, exploring its statistical connection to the indications of the non-Keplerian motion. Based on the astrometric data, we aim to examine whether the flares show statistical significance of the circular non-Keplerian motion around Sgr A*.

The rest of the paper is organized as follows. In Section II, we present the observed data, describe our ray-tracing method for modeling the emission from the hotspot, and outline the setup of parameter estimation in Bayesian framework. Section III details the fitting results using both the averaged and individual flare data, under different orbit configurations. In Section IV, we summarize our findings and provide a discussion of the implications.

II. DATASETS AND METHODS

In this section, we describe the methodology used to model and fit the apparent tracks of flares, including ray tracing and parameter estimation via Markov Chain Monte Carlo (MCMC) sampling. We adopt the hotspot model, in which the observed flares are produced by an orbiting bright spot distributed on the surface of the accretion disks [29, 40, 46]. Specifically, because smaller hotspot size tend to yield better fitting results [44], we consider point-like hotspots in this study. Due to the limited amount and low precision of the available data, it seems not possible to constrain the spin of the black hole [25, 26, 45], we consider the Schwarzschild black hole in the subsequent sections.

A. GRAVITY dataset

The data used in this study were published by the GRAVITY Collaboration in 2023 [26] including 6 with polarimetric data and 4 with astrometric data. All astrometric measurements revealed a consistent clockwise motion of the flare centroids on the sky with periods of approximately one hour, accompanied by full rotations of the polarization vector at the same time. The astrometric positions of these flares are located very close to the Galactic Center, within a few Schwarzschild rad. Recent studies suggest that the hotspot may exhibit super-Keplerian motion around Sgr A* [43–45], which is a discrepancy with the conclusion in Ref. [25, 26]. It is noted that GRAVITY Collaboration fitted the flare motion with a Schwarzschild orbital model using averaged data [26]. There is a concern that the use of averaged data may smooth over important details of the flare. In this paper, we therefore study the flare motion using both the averaged astrometric data and the astrometric data from individual four flare events.

B. Hotspot orbital configuration and ray tracing method

In our study, the black hole is located at the center with respect to the observer's position. We consider a spherical black hole, where the metric can be given by

$$ds^2 = -f(r)dt^2 + \frac{dr^2}{f(r)} + r^2(d\theta^2 + \sin^2\theta d\phi^2). \quad (1)$$

The Schwarzschild black hole is considered in this study, where $f(r) = 1 - 2M/r$, because current GRAVITY dataset seems difficult to constrain the black hole spin [25, 45].

The hotspots in circular orbits could be the most promising models, since hotspot can corotate with the accretion disks as suggested in Refs. [25, 26]. Angular velocity of hotspots induced by pure gravitational force is $\omega_K \equiv u^{(\text{cir}),\phi}/u^{(\text{cir}),t} = (m/r_0^3)^{1/2}$. It is consistent with the results in Newtonian gravity, referred as to Keplerian motion. In the case of deviations from Keplerian motion, the four-velocity of hotspots can be rewritten in the following form,

$$u^{(\text{dK})} = \frac{1}{\sqrt{f(r_0) - r_0^2\omega^2}}\partial_t \pm \frac{\omega}{\sqrt{f(r_0) - r_0^2\omega^2}}\partial_\phi \quad (2)$$

where the parameter $\omega/\omega_K > 1$ denotes the super-Keplerian motions, and $\omega/\omega_K < 1$ denotes the sub-Keplerian motions. Additionally, there is a possibility that the indication of non-Keplerian motions might originate from non-circular orbits. Therefore, we also consider the hotspot moving along planar geodesic orbits. In this case, the initial four-velocity can be written as

$$u_0^{(v)} = \sqrt{\frac{1}{f(r_0)} \left(1 + \frac{L^2}{r_0^2}\right)} \partial_t + \frac{L}{r_0^2} \partial_\phi, \quad (3)$$

where L is the angular momentum, and r_0 is the initial radius of the hotspot orbits. In the following analysis, we consider two orbital models: the hotspot is set to move either along a circular orbit or along a geodesic, both confined to the equatorial plane.

Because the flares are much closer to the center black hole, the bending of light caused by gravity can not be neglected in observations [25, 42]. In methodology, the conventional ray-tracing algorithm, often referred to as “backward ray tracing”, traces light rays backward from each pixel on the image plane to their potential emission sources [47–49]. This approach is effective for the sources like accretion disks, but it becomes computationally expensive for small or point-like sources, as most rays might not reach most of the emission region. Since the emission source in our study is assumed to be point-like, we adopt the our developed ray-tracing algorithm in Ref. [40], which determines the light paths based on the given locations of the emission source and the observer. This approach significantly reduces the computational cost. To produce the temporal

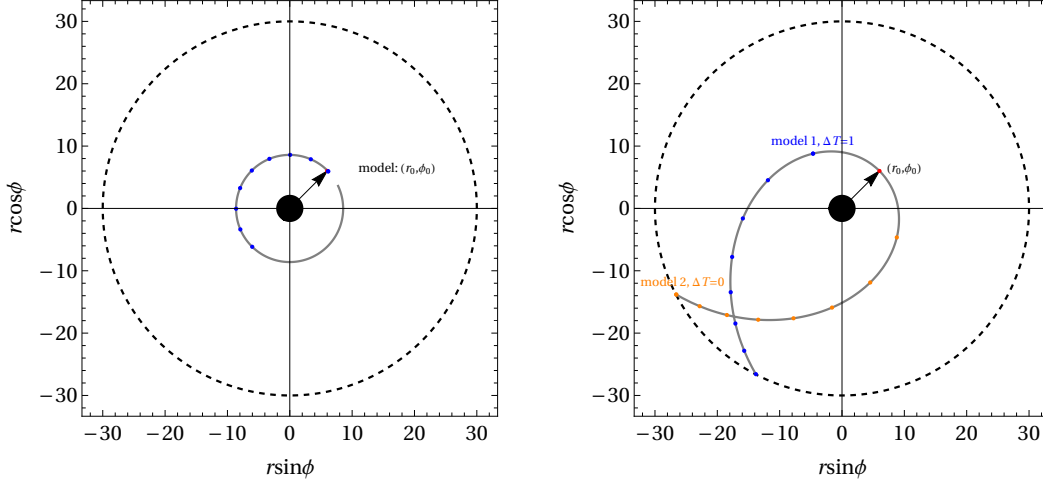


Figure 1: Schematic diagram for illustrating the parameters of hotspots in circular orbits (left panel) and planar geodesic orbits (right panel). The position (r_0, ϕ_0) is the initial position for the circular orbits, and is the innermost point for the planar geodesic orbits. The ΔT formulates the relative distance to the innermost point. The dashed circles represent the boundary of the positions in (r, ϕ) that we studied.

astrometry of the flares, the hotspot track on observers' sky is defined with the flux-weighted centroid position combining the hotspots' primary and secondary images [40, 44].

C. Fitting procedure

We perform the Markov Chain Monte Carlo (MCMC) sampling using the EMCEE method to explore the parameter space in the Bayesian framework. The parameters for circular orbits and planar geodesic orbits are presented as follows,

$$\Theta_{\text{cir}} = (M/M_{\odot}, \theta_{\text{inc}}, r_0/M, \phi_0, \text{PA}, \omega/\omega_k), \quad (4a)$$

$$\Theta_{\text{geo}} = (M/M_{\odot}, \theta_{\text{inc}}, r_0/M, \phi_0, \text{PA}, L/M^2, \Delta T), \quad (4b)$$

where M is the black hole mass, θ_{inc} is the inclination angle of the orbit plane, PA is position angle of the orbit plane projected on the observer's sky, and ω/ω_K is non-Keplerian parameter. The reference positions r_0, ϕ_0 and ΔT for our models are illustrated in the schematic diagram in Fig. 1. We consider the planar geodesic orbits that can reach the innermost point at least once, because the astrometric data have shown a consistent clockwise motion of the flare centroids on the sky [26].

The astrometric data of the flares are given in the form of

$$\Xi = (X_i, Y_i) , \quad (5)$$

where $i=[1, 2, \dots, N]$ is sequential index of data points and N is number of data points. With the model parameters in Eqs. (4) and dataset in the form of Eq. (5), the log-likelihood function is can be given by

$$\mathcal{L}(\Theta_{\text{model}}) = -\frac{1}{2} \sum_{i=1}^N \left(\left(\frac{X_i - X_{\text{model}}(t_i)}{\sigma_{X_i}} \right)^2 + \left(\frac{Y_i - Y_{\text{model}}(t_i)}{\sigma_{Y_i}} \right)^2 \right) , \quad (6)$$

where $X_{\text{model}}(t_i)$ and $Y_{\text{model}}(t_i)$ represent model predictions at time t_i presented in Eqs. (4). The uncertainties σ_{X_i} and σ_{Y_i} follow the values reported in Ref. [26]. We run MCMC sampling using 100 chains, each with 2000 iterations for circular orbits, and 3000 iterations for planar geodesic orbits. And uniform prior distributions are adopted for all the parameters.

III. ANALYSIS OF THE FITTED RESULTS

To investigate the kinematic behavior of the flares, we model the apparent hotspot tracks using ray-tracing simulation with given orbit configuration, and subsequently conduct Bayesian parameter estimation. The best-fit parameters were given by globally optimal ones in the samples. The resulting constraints and corresponding uncertainty on orbital radius, inclination, and other relevant parameters are presented. Physically, we focus on whether the orbits show significant deviations from the circular Keplerian motions.

A. Hotspots in circular orbits

We begin our analysis by considering the case in which the hotspot moves along a circular orbit confined to the equatorial plane. As shown in bottom-left panel of Fig. 2, we used the averaged flare data reported by GRAVITY (2023) [26] and performed parameter estimation for our models. In this case, the black hole mass was treated as a free parameter. The resulting angular velocity is $\omega = 1.13_{-0.42}^{+0.54}$, which does not provide conclusive evidence for super-Keplerian motion of the hotspot. This conclusion is consistent with that of the Ref. [26]. Furthermore, the inferred mass and orbital radius exhibit a negative correlation in 2D contours, which also agrees with the findings of Ref. [26]. In top-right panel of Fig. 2, we present the orbit obtained with the best-fit parameters. Our fitted model seems different from the results reported by the GRAVITY Collaboration (2023)

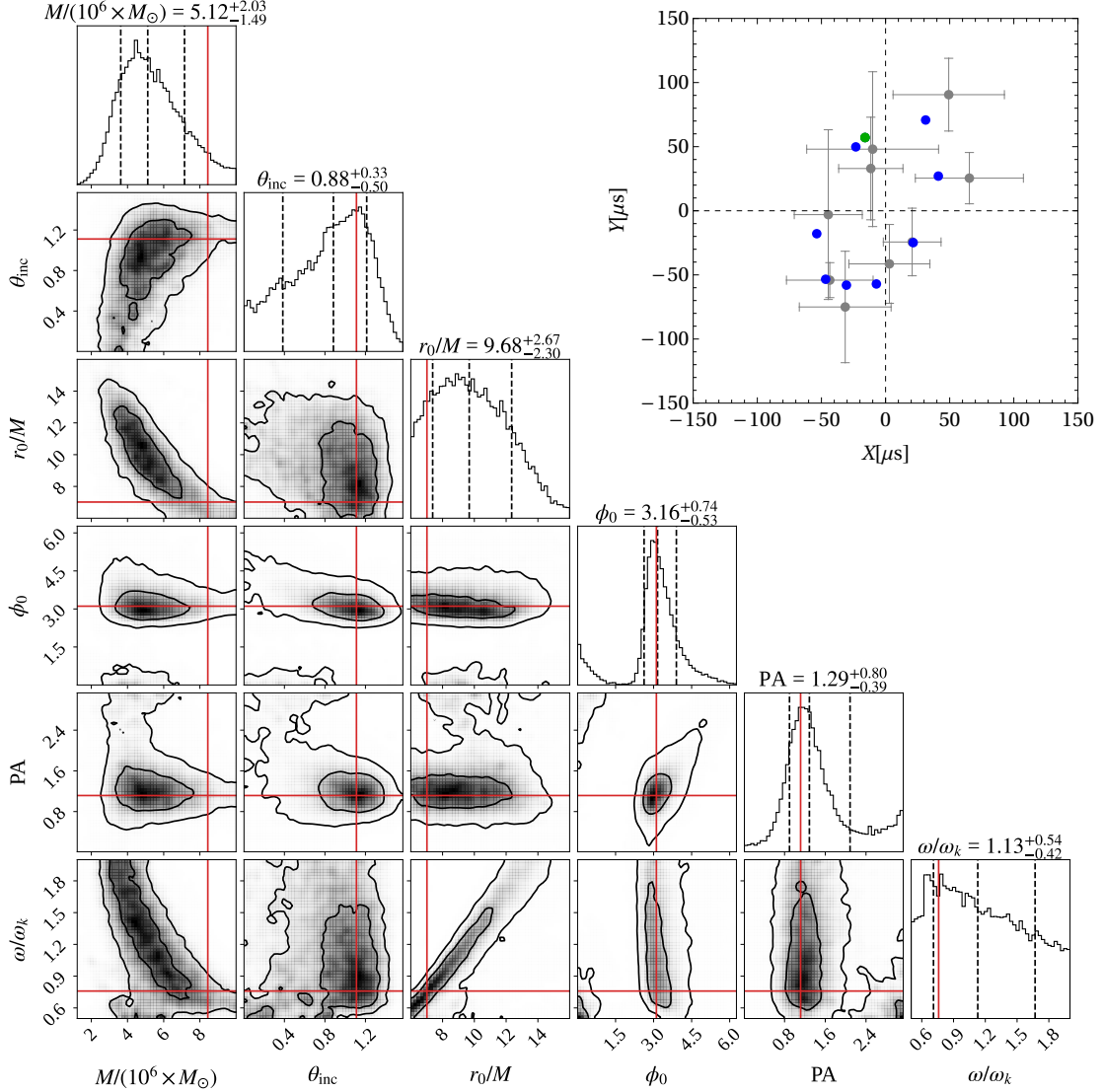


Figure 2: Bottom-left panel: the posterior distributions of model parameters obtained from MCMC sampling for the circular orbit model in the equatorial plane. The red cross marks the globally best-fit parameters. Top-right panel: observed flare centroids (gray points) and the best-fit track (blue points) of a circularly orbiting hotspot in the equatorial plane. We have $\chi^2_{\text{eff}} = 0.18$ for the best-fit parameters.

[26], where the best-fit track looks like a circle. To quantify the goodness of fit, we consider the effective χ^2 as follows,

$$\chi^2_{\text{eff}} = -\frac{2}{2N - N_{\text{d.o.f}}} \mathcal{L}(\Theta_{\text{model}}) . \quad (7)$$

For the results shown in top-right panel of Fig. 2, we have $\chi^2_{\text{eff}} = 0.18$. It yields a lower effective reduced value χ^2_{eff} , compared to pervious studies [26, 45]. However, from the posterior distributions in Fig. 2, the inferred black hole mass seems higher than the well-established value [3, 6]. To address

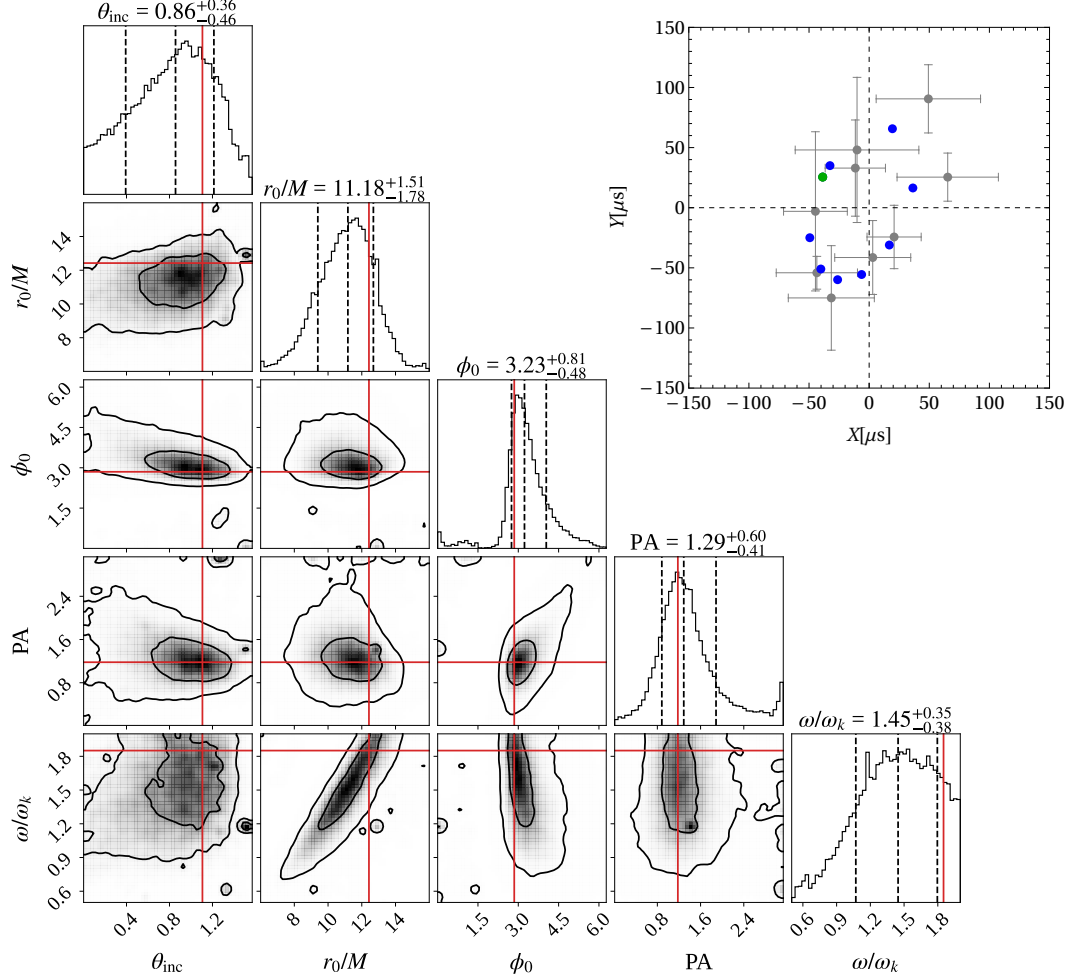


Figure 3: Bottom-left panel: the corner plot for the posterior distributions of model parameters obtained from MCMC sampling for the circular orbit model in the equatorial plane. The red cross marks the globally best-fit parameters. Top-right panel: observed flare centroids (gray points) and the best-fit track (blue points) of a circularly orbiting hotspot in the equatorial plane. Here, the black hole mass M is fixed at $4.3 \times 10^6 M_\odot$ [11]. We have $\chi^2_{\text{eff}} = 0.29$ for the best-fit parameters.

this inconsistency, we fixed the black hole mass at $M = 4.3 \times 10^6 M_\odot$ [11] to preform parameter estimation in bottom-left panel of Fig. 3. In this setup, the inferred non-Keplerian parameter is shown to be $\omega/\omega_k = 1.45^{+0.35}_{-0.38}$, which nearly exceeds unity within the uncertainty range, indicating the possible presence of super-Keplerian motion. From the top-right panel of Fig. 3, the tracks based on the best-fit parameters still agrees well with the observed data, and the resulting reduced $\chi^2_{\text{eff}} (= 0.29)$ value remains low, which suggests a good fit. We summarize the posterior median values of the parameters and corresponding uncertainty in Tab. I.

Table I: Posterior median values and uncertainty of the parameters modeled by hotspot circular orbits with the averaged astrometric data.

Parameter	$M/(M_{\odot} \times 10^6)$	θ_{inc}	r_0/M	ϕ_0	PA	ω/ω_k
Free mass	$5.12^{+2.03}_{-1.49}$	$0.88^{+0.33}_{-0.50}$	$9.68^{+2.67}_{-2.30}$	$3.16^{+0.74}_{-0.53}$	$1.29^{+0.80}_{-0.39}$	$1.13^{+0.54}_{-0.42}$
Fixed mass	4.30 [11]	$0.96^{+0.36}_{-0.46}$	$11.18^{+1.51}_{-1.78}$	$3.23^{+0.81}_{-0.48}$	$1.29^{+0.60}_{-0.41}$	$1.45^{+0.35}_{-0.38}$

B. Analyzing individual astrometric flare data with the circularly orbital hotspots

Since the averaged data might smooth out the details of the hotspot motions, we further investigated individual four flare events to examine the potential presence of the non-Keplerian motion. The posterior distributions for the four flare events are presented in bottom-left Fig. 4. And in Tab. II, we present the posterior median values of the parameters and corresponding uncertainty for the four flare events.

The four flare events yield results that deviate to some extent from those based on averaged data. The flare events on May 27, 2018 and May 19, 2022 indicate the inclination angle tending to be $\pi/2$, while the results of rest of flare events do not. Because the hotspots are assumed to be distributed within one single accretion disk, it leads to some confusion about the validation of the averaged flare astrometry employed in Ref. [26]. From the posterior distributions for the individual flare events, there seems no significant evidence in favor of the non-Keplerian motions. The global best-fit parameters deviate from the posterior median values. It implies that the current data quality and quantity might be insufficient to draw a definitive conclusion regarding the presence of non-Keplerian motion.

We plotted the apparent tracks of hotspots with the best-fit parameters for the four individual flare events, as shown in top-right panels of (a)-(d) in Figs. 4. In chronological order, the χ^2_{eff} for the four flare events are 1.32, 0.90, 3.61 and 0.69, respectively. These values suggest that the circular orbit fits the flares observed on July 22, 2018 and May 19, 2022 particularly well. In contrast, the fits for 27 May and 28 July 2018 exhibit larger deviations, indicating that the simple circular model may not fully capture the flare motions in these cases. While the circular orbit provides a reasonable fit for most flare events, we note that the goodness of fit varies across the four flares. In particular, the 19 May 2022 event yields a lower χ^2_{eff} despite having fewer and less precise data points than the 28 July 2018 event. This suggests that individual flare characteristics and data quality could influence the fitting performance, and some flare, like the event on 19 May 2022, might require more careful modeling.

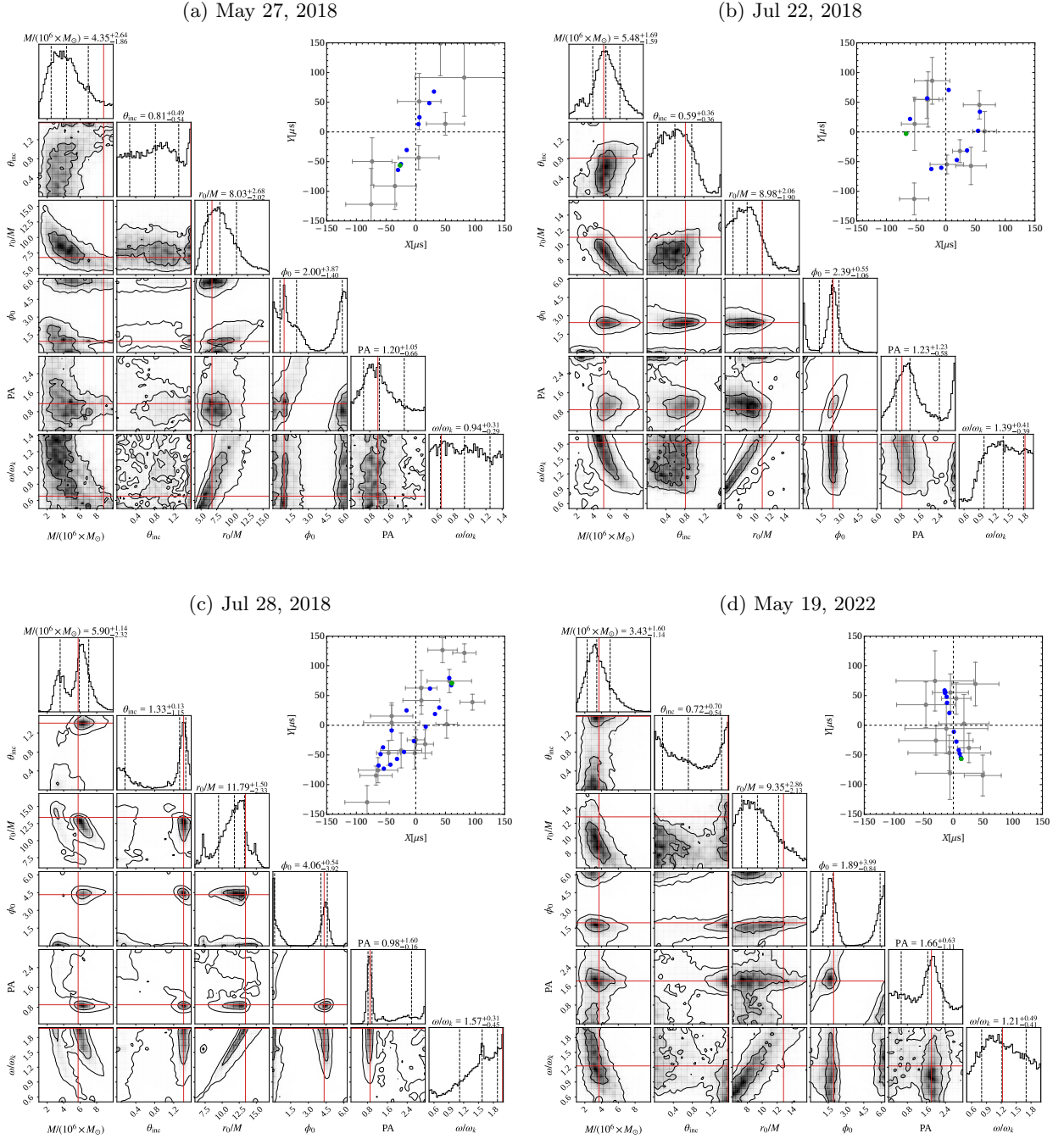


Figure 4: Bottom-left panels of (a)-(d): posterior distributions for the four individual flare events. The red cross marks the globally best-fit parameters. Top-right panels of (a)-(d): corresponding astrometric positions (gray points with error bars) and best-fit tracks (blue points) of a circularly orbiting hotspot for four individual flare events. Each panel corresponds to a flare event reported by the GRAVITY Collaboration. From panels (a) to (d), the corresponding values of χ^2_{eff} are 1.32, 0.90, 3.61 and 0.69, respectively.

Table II: Posterior median values and uncertainty of the parameters modeled by hotspot circular orbits with the four individual astrometric data.

Parameter	27 May 2018	22 Jul 2018	28 Jul 2018	19 May 2022
$M/(M_\odot \times 10^6)$	$4.35^{+2.64}_{-1.86}$	$5.48^{+1.69}_{-1.59}$	$5.90^{+1.14}_{-2.32}$	$3.43^{+1.60}_{-1.14}$
θ_{inc}	$0.81^{+0.49}_{-0.54}$	$0.59^{+0.36}_{-0.36}$	$1.33^{+0.13}_{-1.15}$	$0.72^{+0.70}_{-0.54}$
r_0/M	$8.03^{+2.68}_{-2.02}$	$8.98^{+2.06}_{-1.90}$	$11.79^{+1.50}_{-2.33}$	$9.35^{+2.86}_{-2.13}$
ϕ_0	$2.00^{+3.87}_{-1.40}$	$2.39^{+0.55}_{-1.06}$	$4.06^{+0.54}_{-3.92}$	$1.89^{+3.99}_{-0.84}$
PA	$1.20^{+1.05}_{-0.66}$	$1.23^{+1.23}_{-0.58}$	$0.98^{+1.60}_{-0.16}$	$1.66^{+0.63}_{-1.11}$
ω/ω_k	$0.94^{+0.31}_{-0.29}$	$1.39^{+0.41}_{-0.39}$	$1.57^{+0.31}_{-0.45}$	$1.21^{+0.49}_{-0.41}$

C. Hotspots in planar geodesic orbits

In order to examine the possibility that the non-Keplerian indication could deviate from the non-circular motion, we further fit the flare motions using non-circular geodesic orbits confined to the accretion disks. Fig. 5 presents the posterior distributions for this model. There is no strong anti-correlation between the black hole mass and the orbital radius. With the $\chi^2_{\text{eff}} = 0.14$, the fit remains as good as that of the circular orbit case. In Tab. III, we present the posterior median values of the parameters and the corresponding uncertainty for the planar geodesic orbits.

Because planar geodesic orbits are a generalization of circular Keplerian orbits, we can introduce a circularity parameter to quantify the derviation of non-circular orbits, namely,

$$\gamma \equiv L \sqrt{\frac{2f(r_0) - r_0 f'(r_0)}{r_0^3 f'(r_0)}}. \quad (8)$$

Since we have $L = \sqrt{r_0^3 f'(r_0)/(2f(r_0) - r_0 f'(r_0))}$ for circular orbits, $\gamma = 1$ represents no deviation. Using the posterior distributions of the parameters in Fig. 5, we obtain the posterior distribution of the parameter γ shown in Fig. 6. Our results suggest that circular orbits are preferred among planar geodesic orbits.

Table III: Posterior median values and uncertainty of the parameters modeled by hotspot in planar geodesic orbits with the avaraged astrometric data.

Parameter	$M/(M_\odot \times 10^6)$	θ_{inc}	r_0/M	ϕ_0	PA	L	ΔT
—	$5.84^{+1.68}_{-1.51}$	$1.02^{+0.28}_{-0.47}$	$8.90^{+1.93}_{-1.42}$	$0.04^{+1.70}_{-1.51}$	$1.19^{+0.40}_{-0.36}$	$3.62^{+0.24}_{-0.26}$	$0.43^{+0.28}_{-0.24}$

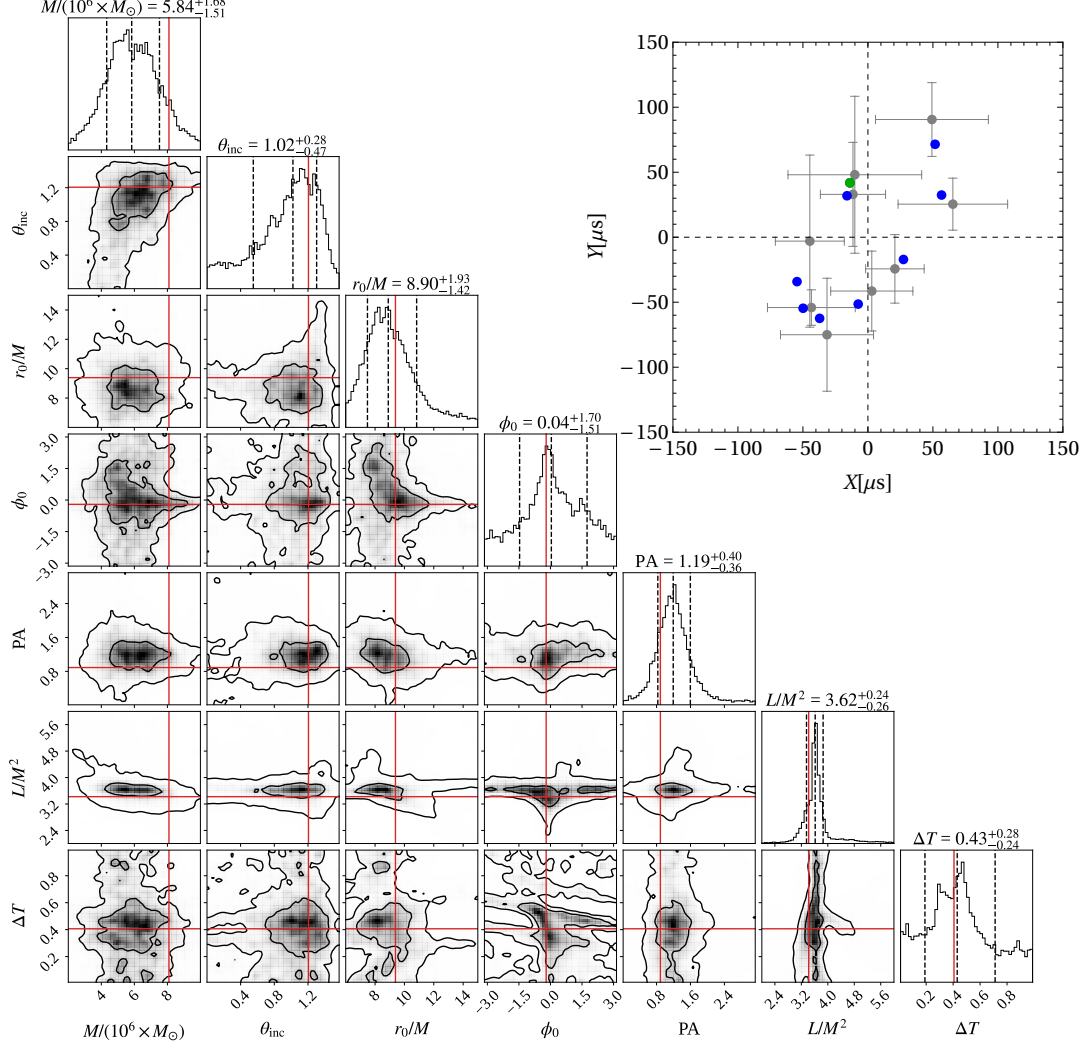


Figure 5: Bottom-left panel: the corner plot for the posterior distributions of model parameters obtained from MCMC sampling for the planar geodesic orbit model. The red cross marks the globally best-fit parameters. Top-right panel: observed flare centroids (gray points) and the best-fit track (blue points) of the orbiting hotspot in the equatorial plane. The value of χ^2_{eff} is 0.14.

IV. CONCLUSIONS AND DISCUSSIONS

In this study, we used the flare data published by the GRAVITY Collaboration in 2023 [26] to investigate the possibility that the flare events exhibit deviations from circular Keplerian motion. For the averaged flare data, when the black hole mass was treated as a free parameter, the resulting hotspot tracks were consistent with circular Keplerian orbits, where $\omega/\omega_k = 1.13^{+0.54}_{-0.42}$, and aligned with the previous study [26]. However, when the black hole mass was fixed at the canonical value of $M = 4.3 \times 10^6 M_\odot$, the fitted tracks tended to favor the super-Keplerian motion at near 1σ confidence level, where $\omega/\omega_k = 1.45^{+0.35}_{-0.38}$.

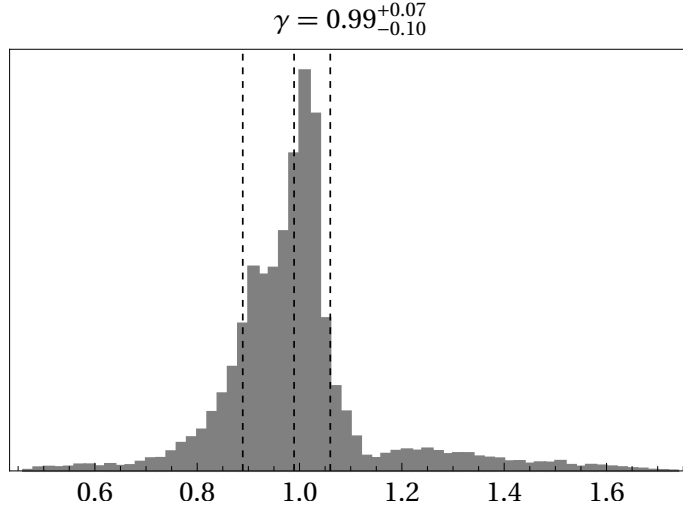


Figure 6: Posterior distribution of the circularity parameter γ .

Since averaging the astrometric data might smooth out critical features of individual flares, we analyzed four individual flare events, separately. In addition, we also explored planar geodesic motion models in an attempt to improve the fits. We summarize the reduced χ^2_{eff} and deviation parameters for hotspots in these orbits in Tab. IV, based on error estimation under the Bayesian framework. For the individual flare data, there seems to be no significant evidence in favor of the non-Keplerian motions. Here, we have ignored the results for the flare on 28 Jul 2018, because of the poorly constrained posterior distribution of ω/ω_k . We also show that the planar geodesic orbits also did not yield a significantly better fit compared to the circular orbits. The orbital circularity parameter is constrained to $\gamma = 0.99^{+0.07}_{-0.10}$. Compared with previous studies [45, 50], our results showed lower reduced χ^2_{eff} values while exhibiting approximately ten times larger uncertainties for the non-Keplerian parameter ω/ω_k , which might be attributed to their use of polarimetric flare data. We conclude that current astrometric flare data alone might be insufficient to definitively determine whether the flares generally exhibit non-Keplerian motion.

As noted by the GRAVITY Collaboration (2020) [44], the observed centroid motions are consistent with circular orbital motion. However, the fitted orbital periods are systematically shorter than those predicted by Keplerian motions. This discrepancy suggests the presence of more complex dynamical effects, possibly pointing toward alternative gravity models or additional forces acting on the orbiting hotspot. The limited flare dataset may obscure more subtle dynamical features, and dataset from the future high-precision observations with the GRAVITY interferometer are expected to offer better constraints on the true nature of the flare motions.

Acknowledgments. This work has been supported by the National Natural Science Fund of

Table IV: Deviation parameters from circular Keplerian motion and effective χ_{eff} from the best fits

Model	data	ω/ω_k	γ	χ_{eff}^2
Circular orbit	Averaged data	$1.13^{+0.54}_{-0.42}$	—	0.18
Circular orbit (fixed mass)	Averaged data	$1.45^{+0.35}_{-0.38}$	—	0.29
Circular orbit	27 May 2018	$0.94^{+0.31}_{-0.29}$	—	1.32
Circular orbit	22 Jul 2018	$1.39^{+0.41}_{-0.39}$	—	0.90
Circular orbit	28 Jul 2018	$1.57^{+0.31}_{-0.45}$	—	3.61
Circular orbit	19 May 2022	$1.21^{+0.49}_{-0.41}$	—	0.69
Non-circular geodesic orbit	Averaged data	—	$0.99^{+0.07}_{-0.10}$	0.14

China (Grants No. 12275034, No. 12347101, and No. 12305073).

-
- [1] B. Bertotti, L. Iess, and P. Tortora, *Nature* **425**, 374 (2003).
 - [2] C. M. Will, *Living Rev. Rel.* **17**, 4 (2014), [arXiv:1403.7377 \[gr-qc\]](#).
 - [3] R. Abuter *et al.* (GRAVITY), *Astron. Astrophys.* **615**, L15 (2018), [arXiv:1807.09409 \[astro-ph.GA\]](#).
 - [4] R. Abuter *et al.* (GRAVITY), *Astron. Astrophys.* **636**, L5 (2020), [arXiv:2004.07187 \[astro-ph.GA\]](#).
 - [5] T. Do *et al.*, *Science* **365**, 664 (2019), [arXiv:1907.10731 \[astro-ph.GA\]](#).
 - [6] M. Grould, F. H. Vincent, T. Paumard, and G. Perrin, *Astron. Astrophys.* **608**, A60 (2017), [arXiv:1709.04492 \[astro-ph.HE\]](#).
 - [7] R. Narayan and E. Quataert, *Nature* **615**, 597 (2023), [arXiv:2303.13229 \[astro-ph.HE\]](#).
 - [8] A. Levis, A. A. Chael, K. L. Bouman, M. Wielgus, and P. P. Srinivasan, *Nature Astron.* **8**, 765 (2024), [arXiv:2310.07687 \[astro-ph.HE\]](#).
 - [9] A. Galishnikova, A. Philippov, E. Quataert, F. Bacchini, K. Parfrey, and B. Ripperda, *Phys. Rev. Lett.* **130**, 115201 (2023), [arXiv:2212.02583 \[astro-ph.HE\]](#).
 - [10] R. Genzel, (2021), [arXiv:2102.13000 \[astro-ph.GA\]](#).
 - [11] R. Abuter *et al.* (GRAVITY), *Astron. Astrophys.* **657**, L12 (2022), [arXiv:2112.07478 \[astro-ph.GA\]](#).
 - [12] R. Genzel, F. Eisenhauer, and S. Gillessen, *Rev. Mod. Phys.* **82**, 3121 (2010), [arXiv:1006.0064 \[astro-ph.GA\]](#).
 - [13] K. Akiyama *et al.* (Event Horizon Telescope), *Astrophys. J. Lett.* **930**, L14 (2022), [arXiv:2311.09479 \[astro-ph.HE\]](#).
 - [14] K. Akiyama *et al.* (Event Horizon Telescope), *Astrophys. J. Lett.* **930**, L12 (2022), [arXiv:2311.08680 \[astro-ph.HE\]](#).
 - [15] V. Perlick and O. Y. Tsupko, *Phys. Rept.* **947**, 1 (2022), [arXiv:2105.07101 \[gr-qc\]](#).
 - [16] S. Vagnozzi *et al.*, *Class. Quant. Grav.* **40**, 165007 (2023), [arXiv:2205.07787 \[gr-qc\]](#).

- [17] Z. Zhang, S. Chen, and J. Jing, *JCAP* **09**, 027 (2024), [arXiv:2404.12223 \[gr-qc\]](#).
- [18] S. Chen and J. Jing, *JCAP* **05**, 023 (2024), [arXiv:2310.06490 \[gr-qc\]](#).
- [19] X.-M. Kuang, Y. Meng, E. Papantonopoulos, and X.-J. Wang, *Phys. Rev. D* **110**, L061503 (2024), [arXiv:2406.11932 \[gr-qc\]](#).
- [20] P.-C. Li, M. Guo, and B. Chen, *Phys. Rev. D* **101**, 084041 (2020), [arXiv:2001.04231 \[gr-qc\]](#).
- [21] Z. Chang and Q.-H. Zhu, *JCAP* **09**, 003 (2021), [arXiv:2104.14221 \[gr-qc\]](#).
- [22] Q.-H. Zhu, Y.-X. Han, and Q.-G. Huang, *Eur. Phys. J. C* **83**, 88 (2023), [arXiv:2205.14554 \[gr-qc\]](#).
- [23] K.-J. He, J.-T. Yao, X. Zhang, and X. Li, *Phys. Rev. D* **109**, 064049 (2024).
- [24] R. Abuter, M. Accardo, A. Amorim, *et al.*, *Astron. Astrophys.* **602**, A94 (2017).
- [25] R. Abuter *et al.* (GRAVITY), *Astron. Astrophys.* **636**, L5 (2020), [arXiv:2004.07187 \[astro-ph.GA\]](#).
- [26] R. Abuter *et al.* (GRAVITY), *Astron. Astrophys.* **677**, L10 (2023), [arXiv:2307.11821 \[astro-ph.GA\]](#).
- [27] I. El Mellah, B. Cerutti, and B. Crinquand, *Astron. Astrophys.* **677**, A67 (2023), [arXiv:2305.01689 \[astro-ph.HE\]](#).
- [28] N. Aimar, A. Dmytriiev, F. H. Vincent, I. E. Mellah, T. Paumard, G. Perrin, and A. Zech, *Astron. Astrophys.* **672**, A62 (2023), [arXiv:2301.11874 \[astro-ph.HE\]](#).
- [29] G. Bao, *Astron. Astrophys.* **257**, 594 (1992).
- [30] Z. Li and C. Bambi, *Phys. Rev. D* **90**, 024071 (2014), [arXiv:1405.1883 \[gr-qc\]](#).
- [31] N. Hamaus, T. Paumard, T. Muller, S. Gillessen, F. Eisenhauer, S. Trippe, and R. Genzel, *Astrophys. J.* **692**, 902 (2009), [arXiv:0810.4947 \[astro-ph\]](#).
- [32] S. D. von Fellenberg *et al.*, *Astron. Astrophys.* **669**, L17 (2023), [arXiv:2301.02558 \[astro-ph.HE\]](#).
- [33] B. Chen, Y. Hou, Y. Song, and Z. Zhang, *Phys. Rev. D* **111**, 083045 (2025), [arXiv:2407.14897 \[astro-ph.HE\]](#).
- [34] J. Huang, Z. Zhang, M. Guo, and B. Chen, *Phys. Rev. D* **109**, 124062 (2024), [arXiv:2402.16293 \[gr-qc\]](#).
- [35] Y. Chen, P. Wang, and H. Yang, *Eur. Phys. J. C* **84**, 270 (2024), [arXiv:2401.10905 \[gr-qc\]](#).
- [36] J. a. L. Rosa, D. S. J. Cordeiro, C. F. B. Macedo, and F. S. N. Lobo, *Phys. Rev. D* **109**, 084002 (2024), [arXiv:2401.07766 \[gr-qc\]](#).
- [37] J. a. L. Rosa, P. Garcia, F. H. Vincent, and V. Cardoso, *Phys. Rev. D* **106**, 044031 (2022), [arXiv:2205.11541 \[gr-qc\]](#).
- [38] H. L. Tamm and J. a. L. Rosa, *Phys. Rev. D* **109**, 044062 (2024), [arXiv:2310.12681 \[gr-qc\]](#).
- [39] J. a. L. Rosa, C. F. B. Macedo, and D. Rubiera-Garcia, *Phys. Rev. D* **108**, 044021 (2023), [arXiv:2303.17296 \[gr-qc\]](#).
- [40] Q.-H. Zhu, *Phys. Rev. D* **111**, 044010 (2025), [arXiv:2411.04001 \[gr-qc\]](#).
- [41] S.-W. Wei, Y.-C. Zou, Y.-P. Zhang, and Y.-X. Liu, *Phys. Rev. D* **110**, 064006 (2024), [arXiv:2401.17689 \[gr-qc\]](#).
- [42] T. Matsumoto, C.-H. Chan, and T. Piran, *Mon. Not. Roy. Astron. Soc.* **497**, 2385 (2020), [arXiv:2004.13029 \[astro-ph.HE\]](#).
- [43] E. Antonopoulou and A. Nathanail, *Astron. Astrophys.* **690**, A240 (2024), [arXiv:2405.10115 \[astro-](#)

- [ph.HE](#)].
- [44] M. Bauböck *et al.* (GRAVITY), [Astron. Astrophys. **635**, A143 \(2020\)](#), [arXiv:2002.08374 \[astro-ph.HE\]](#).
 - [45] A. I. Yfantis, M. Wielgus, and M. A. Mościbrodzka, [Astron. Astrophys. **691**, A327 \(2024\)](#), [arXiv:2408.07120 \[astro-ph.HE\]](#).
 - [46] R. Genzel, F. Eisenhauer, and S. Gillessen, *Rev. Mod. Phys.* **82**, 3121 (2010).
 - [47] F. H. Vincent, T. Paumard, E. Gourgoulhon, and G. Perrin, [Class. Quant. Grav. **28**, 225011 \(2011\)](#), [arXiv:1109.4769 \[gr-qc\]](#).
 - [48] J. Dexter and E. Agol, *Astrophys. J.* **696**, 1616 (2009).
 - [49] J. Dexter, *Mon. Not. R. Astron. Soc.* **462**, 115 (2016).
 - [50] A. I. Yfantis, M. A. Mościbrodzka, M. Wielgus, J. T. Vos, and A. Jimenez-Rosales, [Astron. Astrophys. **685**, A142 \(2024\)](#), [arXiv:2310.07762 \[astro-ph.HE\]](#).